



Unrevealing the thermophysical properties and microstructural evolution of $\text{MgCl}_2\text{-NaCl-KCl}$ eutectic: FPMD simulations and experimental measurements

Xuejiao Li^{a,b,c}, Na Li^{a,b,c}, Weihua Liu^{a,b,c,**}, Zhongfeng Tang^{a,b,c,*}, Jianqiang Wang^{a,b,c}

^a Shanghai Institute of Applied Physics, Chinese Academy of Sciences, Shanghai, 201800, China

^b Key Laboratory of Interfacial Physics and Technology, Chinese Academy of Sciences, Shanghai, 201800, China

^c Dalian National Laboratory for Clean Energy, Dalian, 116023, China

ARTICLE INFO

Keywords:

First principle molecular dynamics
 $\text{MgCl}_2\text{-NaCl-KCl}$ eutectic
 Thermophysical properties
 Structural evolution
 Melting mechanism

ABSTRACT

The first principle molecular dynamics (FPMD) simulations in combination with experimental measurements are applied to investigate the thermophysical properties and structural evolution of $\text{MgCl}_2\text{-NaCl-KCl}$ (MNK) eutectic. The densities, melting point, and enthalpy of fusion simulated by FPMD within NPT ensemble are consistent with experimental results. Besides, the thermal conductivity of molten MNK eutectic evaluated from FPMD simulations with NVT ensemble gives satisfactory result. Furthermore, the shear viscosities of MNK eutectic are deduced based on ion self-diffusion coefficients and solvodynamic radius, similar to the data estimated by additive contribution method. Eventually, the change rules of radial and angular distribution functions and structural factor of MNK eutectic during melting are revealed, and the melting mechanism is proposed from the evolution of polyhedral coordination structures. These results are heuristic in structure-activity relationship of MNK eutectic, which sheds insight for further development of efficient heat transfer and storage media through microstructure engineering.

1. Introduction

Chloride salt mixtures are one of the promising high-temperature heat transfer fluids and heat storage media for the generation III concentrated solar power (CSP) plants due to appropriate melting points, attractive costs, and relatively high energy densities [1–3]. Ternary $\text{MgCl}_2\text{-NaCl-KCl}$ (MNK) eutectic salts possess low melting points, large latent heat densities, good thermal stabilities, and high operating temperatures satisfying the criterion of candidate materials for CSP [4]. Experimentally, Mohan et al. determined the melting point, heat capacity, and mass loss of MNK with a eutectic composition of 55.0–24.5–20.5 wt% [5], and Sun et al. investigated the corrosion behavior of Fe- and Ni-based alloys in molten MNK with the same composition [6]. Ding et al. also studied the hot corrosion behavior of multiple commercial alloys in molten MNK (3:1:1 mol %) under inert atmosphere [7,8], and Yuan and Vandarkuzhali et al. demonstrated the electrochemical behavior of metal oxides in molten MNK eutectic (5:3:2 mol%) [9,10]. However, the known and reliable data of density, thermal

conductivity, and shear viscosity of MNK eutectic are scarce due to the difficulties in measurement at high-temperature, anhydrous and anaerobic environment.

Theoretically, the semi-empirical and ab-initio calculation approaches were applied to examine thermodynamic modelings, to study atomic-level interactions, and to evaluate thermophysical properties of chloride salts and their mixtures [11,12]. Robelin et al. optimized the thermodynamic database of MNK-based chlorides by using FactSage in conjunction with Gibbs free energy minimization software [13], Galamba et al. calculated the thermal conductivities and shear viscosities of molten NaCl and KCl, respectively, through equilibrium molecular dynamics (EMD) simulations with Born-Mayer-Huggins-Tosi-Fumi (BMHTF) rigid-ion potential [14,15], and Wang et al. simulated the transport properties and local structures of mono- and binary molten alkali chlorides by classical molecular dynamics [16,17]. However, the microstructural, thermodynamic and kinetic simulations of MNK eutectic have not been reported in literatures due to the shortage of effective force fields for MgCl_2 . Therefore, the first principles molecular

* Corresponding author. Shanghai Institute of Applied Physics, Chinese Academy of Sciences, Shanghai, 201800, China.

** Corresponding author. Shanghai Institute of Applied Physics, Chinese Academy of Sciences, Shanghai, 201800, China.

E-mail addresses: lixuejiao@sinap.ac.cn (X. Li), liuweihua@sinap.ac.cn (W. Liu), tangzhongfeng@sinap.ac.cn (Z. Tang).

dynamics (FPMD) simulations stood out, which calculate the interionic forces from first principles on-the-fly and thus avoid using empirical force field models. In fact, a comparative investigation of molten NaCl had been carried out by EMD and FPMD, indicating that FPMD simulations using Troullier-Martins pseudopotentials provided the most reliable descriptions of structural characteristics and transport properties [18].

In this work, the FPMD simulations are conducted to evaluate thermophysical properties (density, heat capacity, enthalpy of fusion, diffusion coefficient, and thermal conductivity) of MNK eutectic, to compare with corresponding experimental results measured by high-temperature densitometer, differential scanning calorimetry instrument, and thermal diffusivity meter, and to discuss the possible sources of error between FPMD results and experiments to validate the potential applications of FPMD simulations in database establishment for CSP. Besides, the structural characteristics during melting process of MNK eutectic including radial and angular distribution functions, and static structural factors are also analyzed. Especially, the melting mechanism of MNK eutectic is elaborated from the evolution of polyhedral coordination structures, and the interplay between microstructure and viscosity property is revealed.

2. Methodology and technological details

2.1. Computational methods

FPMD are employed in the simulations of MNK eutectic based on density functional theory and Born-Oppenheimer approximation as implemented in the Vienna Ab-Initio Simulation Package (VASP) [19–21]. The simulated MNK system is composed of 19 MgCl₂, 14 NaCl, and 9 KCl corresponding to a molar ratio of 45.37: 32.96: 21.67 mol%, whose mass fraction is same to that of experimental formula salt [5,6]. The generalized gradient approximation (GGA) with the Perdew-Burke-Ernzerhof (PBE) exchange-correlation functional is used for all simulations [22]. The wave functions for valence electrons, Na (2s¹), K_sv(3s²3p⁶4s¹), Mg(3s²) and Cl(3s²3p⁵), are expanded using the plane wave basis set with a cutoff energy at 450 eV [23], and the core electrons are approximated by pseudopotentials developed using the projector augmented wave method [24]. Besides, a 1 × 1 × 1 k-point mesh is chosen in the FPMD simulations considering it is a suitable compromise between computational accuracy and cost [25]. Spin polarization is applied for all FPMD simulations to properly describe the unpaired electrons in valent shells, and to ensure the stability of magnetic moments.

The initial configuration of MNK eutectic above melting point is constructed by randomly inserting method whose model size depends on experimental density, and then the MNK eutectic is cooled down from molten states to solid states. The detailed simulation process is as follows: First, 10000 steps of simulations are carried out using the NVT ensemble with a Nosé thermostat to bring the system to the specified temperatures [26,27]. The integration time step is set to 1 fs with energy drift less than 1 meV per atom per picosecond (ps) for MNK eutectic. Then, another 4000 steps of simulations are conducted in NPT ensemble with an step time of 3 fs to fast optimize cell volumes using Langevin thermostat by the method of Parrinello and Rahman integrated in VASP [28]. The equilibrium cell volume is evaluated from the average of last 3000 steps and used as input of the following NVT simulations. Finally, the reproductive FPMD simulations within NVT ensemble are conducted for 15 ps (5000 steps). All of the structural, thermodynamic and kinetic properties are evaluated after the preparation FPMD simulations at six preset temperatures at 823, 773, 723, 673, 623, and 573 K.

2.2. Experimental methods

The MgCl₂ (analytical purity: >99.9%, Aladdin Co. Ltd), NaCl, and KCl (analytical purity: >99.9%, Sinpharm Chemical Reagent Co. Ltd)

powders are used after separately drying at 150 °C under Ar atmosphere for 48 h, and then melt mixed in a weight ratio of 54.95: 24.50: 20.55 wt % in a graphite crucible at 873 K for 10 h to get the homogeneous eutectic. All experimental operations are conducted in glove box covered with high-purity Ar atmosphere, where H₂O and O₂ contents are maintained below 0.1 and 10.0 ppm, respectively. The density of molten MNK eutectic is measured with the self-developed densitometer based on the Archimedes technique, and the technical details are shown in Ref. [29]. Besides, the melting point, enthalpy of fusion, and specific heat capacity of MNK eutectic are determined by differential scanning calorimetry (DSC Netzsch 404 F3) at a heating rate of 10 K min⁻¹ from 553 to 693 K, with Ar gas protection and 30.0 mL min⁻¹ flow rate of purge [30]. Furthermore, the specific heat capacity is three-step tested by the standard methods as described in ASTM E1269. A baseline heat flow curve is first determined using empty graphite crucibles, followed by the measurement of a standard sapphire reference (supplied by Netzsch), and then the heat flow curve of MNK eutectic is measured. In addition, the laser flash method is applied to measure thermal diffusivity of molten MNK eutectic salt with Linseis LFA 1000, and the data is analyzed by the LFEAuto1061 program considering heat loss and infinite pulse time [31,32].

3. Results and discussion

3.1. Evaluations of thermodynamic properties

3.1.1. Melting point and density

The melting point (T_m) is of critical importance when analyzing phase transition behavior of a mixed salt, in FPMD simulations, the most common method of studying T_m is to simulate system volume as a function of temperature [33,34]. Fig. 1 shows the equilibrium cell parameters (a) and calculated densities (ρ) of MNK eutectic at six temperatures within NPT ensemble. It is noted that the equilibrium temperatures (577, 597, 615, 700, 754, and 797 K) are distinguished from preset temperatures (in Section 2.1) with an average deviation of 3.71%, and the temperature difference of 673 K is up to 58 K implying a prominent structural change of MNK eutectic at this point. Besides, a increases and ρ decreases as temperature (T) increases, and the abrupt changes of a and ρ occur over a small temperature interval of 615–700 K. That is a sign of a transition from solid to liquid, and thus the T_m of 657 K is evaluated from the middle temperature of phase transition region. In Fig. 2, the second heating and cooling cycle curve (total 3 cycles) for a MNK sample analyzed by DSC instrument are depicted, and experimental T_m is taken from the onset point in heating phase. The measured T_m of 656 K (383 °C) is same with that obtained from FPMD, greatly consistent with FactSage prediction and other experimental result [5].

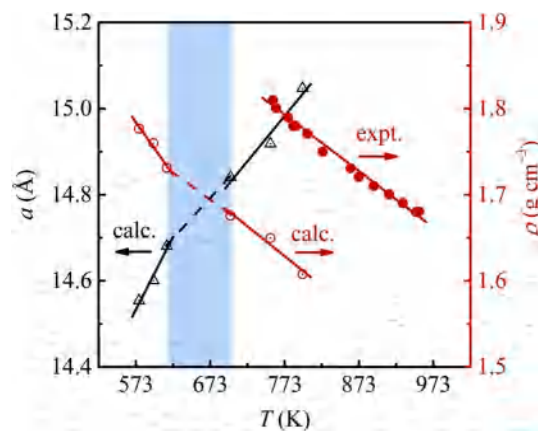


Fig. 1. Calculated cell parameter a , calculated and experimental density ρ of MNK eutectic from FPMD simulations and high-temperature densitometer (the solid lines are the fitted curves and dotted lines are guide to the eyes).

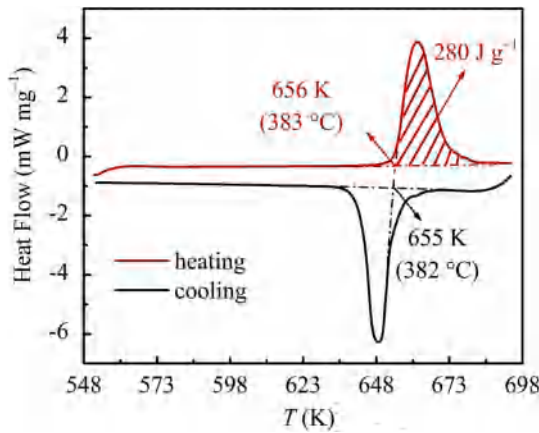


Fig. 2. DSC analysis of MNK eutectic from 553 to 693 K.

From Fig. 1, the simulated α and ρ change approximately linearly with T before 615 K and after 700 K indicating one solid and one liquid configuration, respectively. The relationship equations of ρ and T below 615 K and above 700 K are evaluated as,

$$\rho_s = 2.481 - 1.220 \times 10^{-3} T \quad (T = 577 \sim 615 \text{ K}) \quad (1a)$$

$$\rho_l = 2.165 - 6.938 \times 10^{-4} T \quad (T = 700 \sim 797 \text{ K}) \quad (1b)$$

Besides, the ρ of molten MNK eutectic is also experimentally measured as shown in Fig. 1, and the ρ as a function of T is obtained as,

$$\rho_{\text{expt}} = 2.269 - 6.216 \times 10^{-4} T \quad (T = 757 \sim 955 \text{ K}) \quad (1c)$$

It is shown that the simulated ρ of 1.676 and 1.650 g cm⁻³ at 754 and 797 K are slightly lower than corresponding experimental values of 1.800 and 1.774 g cm⁻³ from Eq. (1c), suggesting the employed pseudopotentials slightly underestimate ionic interactions resulting in increases of cell volumes. In addition, the density of MNK eutectic decreases as temperature increases, agree with the literature results of other MNK melt [35].

3.1.2. Enthalpy of fusion and specific heat capacity

The enthalpy of fusion (ΔH^f) is directly related to the potentials of heat transfer and storage of a salt, which is a latent energy to change a substance from solid to liquid under atmospheric pressure. As shown in Table 1, the T_p and T_v represent equilibrium temperatures obtained from FPMD simulations within NPT and NVT ensembles, respectively. The total energies (E_p and E_v) of MNK eutectic for multiple temperatures at isothermal-isobaric and isothermal-isometric conditions are also listed, and the relative energies (ΔE_p and ΔE_v) are calculated by designing a thermodynamic cycle and comparing with the absolute E_p and E_v at 0 K. The ΔH^f of MNK eutectic is directly related to ΔE_p and can be expressed as,

$$\Delta H_p^f = \frac{\Delta E_p N_A}{NM} \quad (2)$$

where N_A is the Avogadro constant, N the atomic number (103) and M the average mole mass (78.53 g mol⁻¹) of MNK simulation system. Eventually, the average ΔH_p^f of 282.77 J g⁻¹ is evaluated based on the average value of ΔE_p (22.93 and 24.48 eV) when T is definitely higher than T_m , and it agrees well with 280 J g⁻¹ obtained from the integral area of DSC heating curve (in Fig. 2) and literature value of 284 J g⁻¹ [36].

The specific heat capacity (c) is an important factor to evaluate many emergency scenarios, which is a measurement of how much energy is required to change system temperature. In FPMD simulations, the c is usually evaluated by Eq. (3) from the fluctuation method of free energy [37].

$$c = \frac{N_A}{Mk_B T^2} (\langle F^2 \rangle - \langle F \rangle^2) \quad (3)$$

where F is Gibbs free energy of a system without entropy, k_B is Boltzmann constant, and $\langle \dots \rangle$ is ensemble average of the last 3000 steps obtained from FPMD simulations. Therefore, the isobaric and isometric specific heat capacity (c_p and c_v) of MNK eutectic are estimated as summarized in Table 1. The average c_p of solid MNK salt is evaluated as 1.825 J g⁻¹ K⁻¹, while the c_p of molten MNK (5.687 J g⁻¹ K⁻¹) is significantly larger than that of solid state. As shown in Fig. 3, the c_p of MNK eutectic is measured by DSC from 373 to 873 K, and the average c_p of molten MNK (1.140 J g⁻¹ K⁻¹) is greater than that of solid MNK (0.936 J g⁻¹ K⁻¹). These experimental results are similar to the literature data [5], however, both of them are lower than FPMD results. In addition, the c_p of molten MNK is slightly decreases as temperature increases, and the change trend is opposite to that of FPMD simulations. The insufficient specimens including initial configurations and simulation steps result in the overestimates of c_p values about 2–5 times, which is

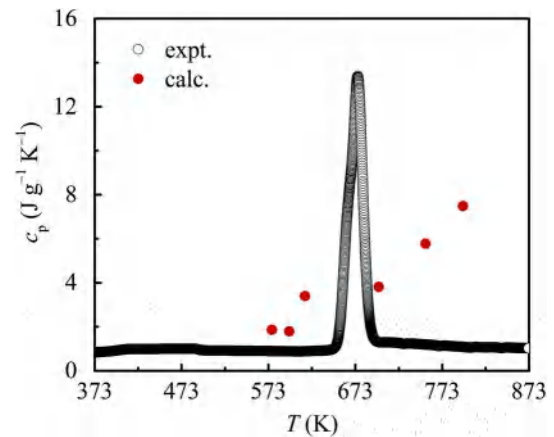


Fig. 3. Experimental and calculated specific heat capacities of MNK eutectic.

Table 1

Equilibrium temperature (T_p and T_v , unit: K), total and relative energy (E and ΔE_p , unit: eV), enthalpy of fusion (ΔH_p^f and ΔH_v^f , unit: J g⁻¹), and specific heat capacity (c_p and c_v , unit: J g⁻¹ K⁻¹) of MNK eutectic simulated by FPMD within NPT and NVT ensembles.

T_p	E_p	ΔE_p	ΔH_p^f	c_p	T_v	E_v	ΔE_v	ΔH_v^f	c_v
797	-325.14	24.48	292.03	7.48	823	-333.37	22.70	270.77	25.67
754	-326.69	22.93	273.51	5.77	773	-333.49	22.58	269.34	28.58
700	-328.37	21.25	253.45	3.81	723	-335.99	20.08	239.52	26.91
615	-331.83	17.79	212.16	3.39	673	-339.34	16.73	199.60	11.16
597	-332.71	16.91	201.73	1.79	623	-340.57	15.50	184.95	9.10
577	-333.31	16.30	194.48	1.86	573	-340.95	15.12	180.37	11.24
0	-349.62	0.00	0.00	-	0	-356.07	0.00	0.00	-

seriously limited by the computational cost of FPMD simulations. On the other hand, the ideality of simulation system within NPT ensemble and the smaller model cell consisting of 103 atoms far away from the macro system lead to the differences of change rule, especially at high temperature.

3.2. Evaluations of kinetic properties

3.2.1. Ionic self-diffusion coefficient

Ionic self-diffusion coefficient (D) can be evaluated from the long-time slope of the mean-squared displacement (MSD) on the basis of the Einstein formula [38].

$$D = \frac{1}{6} \lim_{\tau \rightarrow \infty} \frac{d}{d\tau} \left\langle \sum_i \delta \mathbf{r}_i(\tau)^2 \right\rangle \quad (4)$$

where $\delta \mathbf{r}_i(\tau)$ is the displacement of the same ion i after a time delay of τ , and the summation is over all i ions in MNK eutectic. Fig. 4 shows the sum of MSDs of ions at six temperatures presenting good linear relationship with time, and the total D is evaluated from the simulation time of 1 ps–14 ps as shown in Table 2. As far as we know, there is no research on the D of molten MNK, but the D of molten NaCl can be as a reference. The experimental D_{Na^+} and D_{Cl^-} of molten NaCl are 2.0×10^{-4} and $1.7 \times 10^{-4} \text{ cm}^2 \text{ s}^{-1}$ at a temperature range of 1528–1539 K, respectively, which are larger than that of molten MNK at 823 K about one order of magnitude [18]. From Table 2, it can be found that the order of diffusion of molten MNK is $D_{\text{Na}^+} > D_{\text{K}^+} > D_{\text{Cl}^-} > D_{\text{Mg}^{2+}}$ which is affected by ionic radius, charge number and ion interaction. However, the rule is not suitable for solid and quasi-liquid MNK eutectics at 573–673 K, in which the relationship of D_{Na^+} and D_{K^+} is changed with temperature. Especially for the MNK system at 673 K, the total D (D_{tot}) is surprisingly smaller than that at 623 K suggesting a possible solid-liquid miscible structure near melting point hampers ion transport in some degree.

In addition, the average thermal diffusivity (D_{thermo}) of molten MNK eutectic is obtained by sampling more than 10 times at each equilibrium temperature as shown in Fig. 5 to reduce systematic and random errors, and the detailed experimental procedure and results are supplemented in section S2 in the supporting information. It should be noted that the D_{thermo} is very dispersive when the temperature at 753 K, a small amount of salt is volatilized sticking to the wall of crucible in experiments, and thus the experimental data after 723 K are not accurate enough. Eventually, the average D_{thermo} of molten MNK at 663, 693, and 723 K are estimated as 3.14×10^{-3} , 3.04×10^{-3} and $3.12 \times 10^{-3} \text{ cm}^2 \text{ s}^{-1}$, respectively. In Table 2, the D_{thermo} is an order of magnitude larger than corresponding D_{tot} evaluated from FPMD simulations, which is caused by the lower jump frequencies of ions due to shorter simulation times

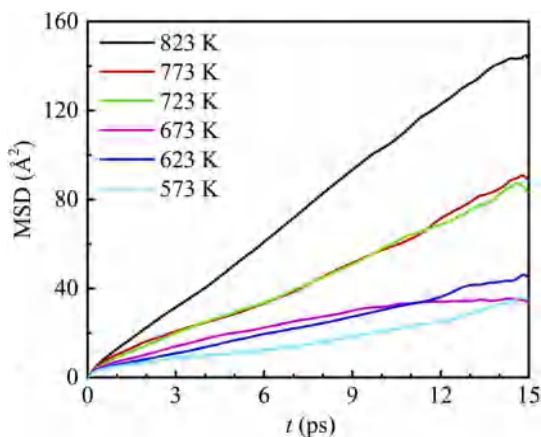


Fig. 4. Mean-squared displacement (MSD) of MNK eutectic at multiple temperatures simulated by FPMD within NVT ensemble.

Table 2

Ionic self-diffusion coefficients (D , unit: $10^{-5} \text{ cm}^2 \text{ s}^{-1}$), thermal conductivity (λ , unit: $\text{W K}^{-1} \text{ m}^{-1}$), and shear viscosity (η , unit: cP) of MNK eutectic from FPMD simulations within NVT ensemble.

T	$D_{\text{Mg}^{2+}}$	D_{Na^+}	D_{K^+}	D_{Cl^-}	D_{tot}	λ	η
823	1.99	8.13	3.74	2.95	16.81	0.694	1.289
773	1.00	5.13	1.91	1.33	9.36	0.441	2.151
723	0.71	3.77	3.20	1.51	9.19	0.414 ^a	2.090
673	0.65	1.13	1.20	0.83	3.81	0.074	4.734
623	0.44	2.31	1.31	0.71	4.77	0.076	3.422
573	0.17	1.12	1.54	0.36	3.20	0.064	4.746

^a experimental thermal conductivity at 723 K is $0.712 \text{ W K}^{-1} \text{ m}^{-1}$.

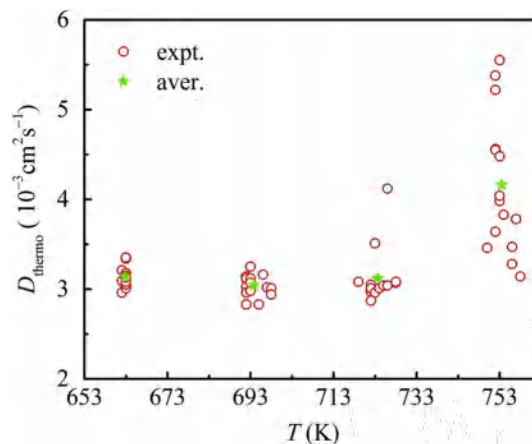


Fig. 5. Experimental and average thermal diffusivities (D_{thermo}) of molten MNK eutectic.

and fewer ionic numbers.

3.2.2. Thermal conductivity

The assessment of thermal conductivity (λ) is of great importance, a larger λ increases cooling effect of heat exchangers avoiding large temperature gradients within molten salt and non-uniformities in criticality and power production. In molten salt systems, the λ itself has a weak temperature dependence, which accounts for how much energy flows through a surface in the system. Usually, λ can be deduced from the following equation,

$$\lambda = D_{\text{thermo}} c_p \rho \quad (5)$$

Therefore, the λ is indirectly evaluated according to above experimental D_{thermo} , c_p and ρ , and the average λ values of molten MNK at 663, 693, and 723 K are 0.838, 0.748 and $0.712 \text{ W K}^{-1} \text{ m}^{-1}$ as shown in Table S3, respectively. Similarly, the FPMD λ of MNK eutectic can also be evaluated according to Eq. (5), where c_p and D_{thermo} are replaced by c_v and D_{tot} considering a better temperature controlling of Nosé thermostat. As shown in Table 2, the λ of solid MNK eutectic is almost constant with an average value of $0.071 \text{ W K}^{-1} \text{ m}^{-1}$, which is greatly lower than of molten MNK eutectic. However, the simulated λ of molten MNK eutectic slightly increases with temperature increasing from 723 to 823 K, and the λ of $0.414 \text{ W K}^{-1} \text{ m}^{-1}$ at 723 K is lower than the corresponding experimental value at the same temperature. The average value of simulated λ of molten MNK eutectic ($0.516 \text{ W K}^{-1} \text{ m}^{-1}$) agrees well with experimental value.

3.3. Quantitative structure-activity relationship

3.3.1. Radial and angular distribution functions

The radial distribution functions (RDFs) of molten salts can be measured experimentally using neutron scattering and X-ray diffraction

techniques, allowing us to benchmark how well our simulations reproduce the molten MNK eutectics. Fig. 6a shows the RDFs and their integral functions of Mg–Cl, Na–Cl, K–Cl, and Cl–Cl ion pairs at 823 K, respectively. It can be seen the peak of Mg–Cl is significantly higher and sharper than that of Na–Cl and K–Cl, depending on the higher concentration of MgCl₂ and stronger interaction between Mg²⁺ and Cl⁻. The peak heights of Na–Cl (3.7) and Cl–Cl (2.0) agree well with the experimental and simulation values of 3.3–3.9 and 1.7–1.9 in molten NaCl [18]. Besides, the nearest neighbor distances of Na–Cl and Cl–Cl are 2.708 Å and 3.697 Å, respectively, consistent with literature values of 2.6 and 3.8 Å at 1148 K [18]. The first peak positions of Mg–Cl and K–Cl are 2.357 and 3.102 Å which are also comparable with corresponding results in molten ZnCl₂–NaCl–KCl simulated by classical MD [39,40].

In addition, the proportions of coordination number (CN) of four ion pairs at 823 K are 72.46%, 76.73%, 87.39% and 54.39% with a cutoff distance of 4.0 Å, and the average CNs of cation-anion in first shell are 4.60, 5.51 and 6.23, respectively. The analysis reveals that the Cl⁻ distribution around Mg²⁺ is similar to that of Zn²⁺ which shows a tetrahedral coordination in molten ZnCl₂–NaCl and ZnCl₂–NaCl–KCl mixtures [39,40]. In Table 3, The first peak positions and CNs of three cation-anion pairs and four homogeneous ionic pairs at six temperatures are summarized. Furthermore, the angular distribution functions (ADF) reflecting bond orientation of MNK eutectic are depicted in Fig. 6b [41]. It is shown that the span of four angels is from 40° to 180°, and ∠Cl–Mg–Cl, ∠Cl–Na–Cl, ∠Cl–K–Cl and ∠Cl–Cl–Cl with maximum distributions are 93°, 75°, 69°, and 61°, respectively. The monovalent cations of Na and K exhibit similar angular distribution, however, there is another small peak for ∠Cl–Mg–Cl at 162° verifying the polyhedral arrangement structures of Cl ions bridged Mg ions. As shown in the inset of Fig. 6b, a partial snapshot of molten MNK eutectic is captured with the

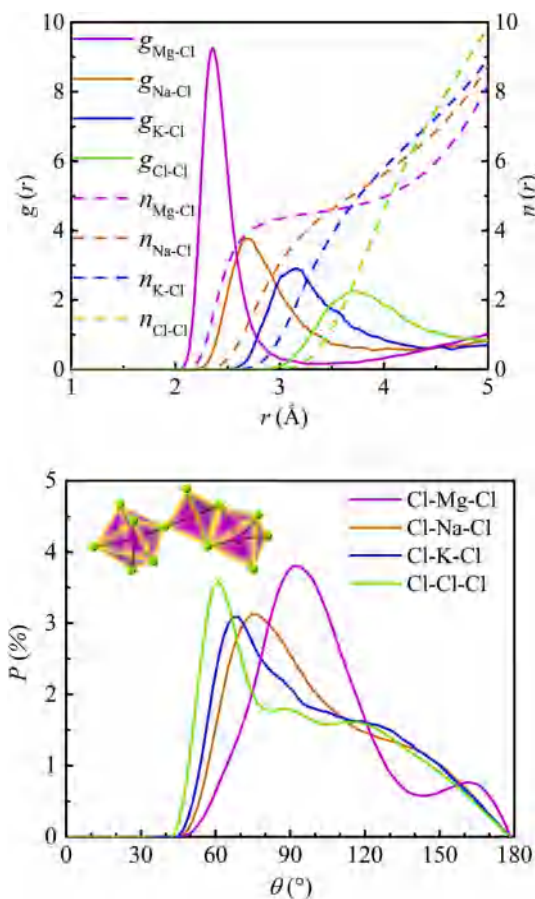


Fig. 6. (a) Radial and (b) angular distribution functions (RDFs and ADFs) of molten MNK eutectic at 823 K by FPMD simulations.

Table 3

First peak positions and coordination numbers (in bracket) of ionic pairs in MNK eutectic by FPMD simulations within NVT ensemble.

T	Mg–Cl	Na–Cl	K–Cl	Cl–Cl	Mg–Mg	Na–Na	K–K
823	2.357 (4.60)	2.708 (5.51)	3.102 (6.23)	3.697 (9.61)	3.772 (2.17)	4.176 (3.98)	5.421 (3.30)
773	2.358 (4.59)	2.695 (5.64)	3.149 (6.41)	3.708 (9.89)	3.761 (2.27)	4.510 (3.86)	5.354 (3.02)
723	2.366 (4.69)	2.671 (5.61)	3.143 (6.59)	3.720 (10.08)	3.752 (2.52)	4.308 (3.53)	4.958 (3.01)
673	2.372 (4.78)	2.694 (5.67)	3.151 (6.77)	3.680 (10.41)	3.690 (2.56)	4.344 (3.54)	4.625 (3.10)
623	2.380 (4.90)	2.679 (5.83)	3.154 (6.72)	3.629 (10.61)	4.011 (2.87)	4.166 (4.12)	5.281 (3.59)
573	2.382 (4.96)	2.732 (5.78)	3.123 (6.99)	3.617 (10.64)	3.864 (3.05)	4.214 (3.75)	4.996 (3.52)

Mg–Cl cutoff distance of 2.910 Å, where a tetrahedral structure by Mg-centered Cl cluster is indeed alternatively bridged by a corner-sharing octahedron and an edge-sharing hexahedron.

3.3.2. Shear viscosity and microstructure

Shear viscosity (η) as one of important thermophysical properties is critically sensitive to diffusion coefficient and microstructure, which dictates what types of pipes and pumps must be used when circulating salt through the operation core and heat exchangers. Usually, the η could be evaluated from the Stokes-Einstein equation during FPMD simulations [42].

$$\eta = \frac{k_B T}{2\pi \bar{D} R_s} \quad (6a)$$

$$R_s = \frac{d_{\text{Na-Na}} + d_{\text{Mg-Mg}} + d_{\text{K-K}} + d_{\text{Cl-Cl}} + 2d_{\text{Cl-Na}} + 2d_{\text{Cl-K}} + 2d_{\text{Cl-Mg}}}{10} \quad (6b)$$

In Eq. (6a), the \bar{D} is the arithmetic mean of $D_{\text{Mg}^{2+}}$, D_{Na^+} , D_{K^+} , and D_{Cl^-} as shown in Table 2. Based on the above discussion, the mass motion in MNK involves cooperative displacements of cations and anions, rather than hopping of single ion from one site to the next. Thus, the R_s is thought as solvodynamic mean radius whose expression in MNK eutectic refers the literature's combination rule [25,43]. In Eq. (6b), all d values are equal to the corresponding first shell coordination distances obtained from RDFs as summarized in Table 3, and the evaluated η from FPMD simulations are also listed in Table 2. It can be seen that the simulated η of molten MNK (1.289–2.151 cP) slightly lower than of 2.597–4.495 cP evaluated by additive contribution method from viscosities of single molten NaCl, KCl, and MgCl₂ [44]. Besides, the η of MNK eutectic at 673 K is obviously greater than that of 623 K, indicating that the unique solid-liquid blends result in the increase of viscosity and thus decrease of diffusivity.

3.3.3. Structural evolution of melting

From Table 3, It can be seen that the structural change from 673 K to 723 K is especially obvious, and the average first peak positions of Mg–Cl, Na–Cl, and K–Cl before and after melting decrease about 0.88%, 0.12%, 0.58%, respectively, while the Cl–Cl coordination distance decreases about 2.01%. Besides, the CNs of cation-anion decrease after melting, suggesting that the polarization effect of heterologous ions in molten MNK is strengthened by temperature. In addition, the static structure factors $S(q)$ is used to study the organization of particles during melting process as shown in Fig. 7. From Fig. 7, the peak positions of simulated neutron and X-rays $S(q)$ at different temperatures are similar to each other, where the first positions are from 2.020 to 2.075 Å⁻¹ and from 2.095 to 2.148 Å⁻¹, respectively, and the second peak positions of neutron $S(q)$ are slightly larger than that of X-rays. Besides, the position of first valley of $S(q)$, especially for the neutron scattering curves, varies from 1.326 to 1.379 Å⁻¹ corresponding to the global first valley of RDFs (4.556–4.738 Å). Overall, all peak positions slightly left-shift as

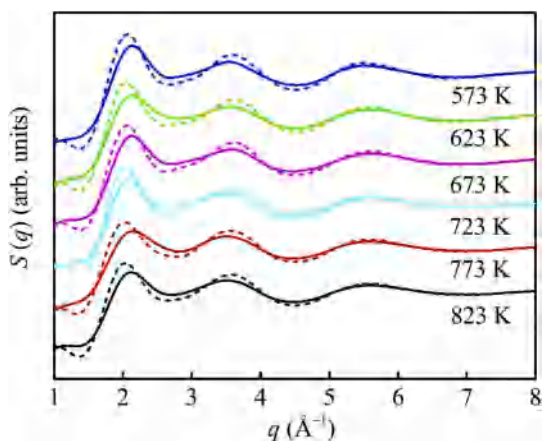


Fig. 7. Static structural factors $S(q)$ of MNK eutectic at multiple temperatures by FPMD simulations (solid line: X-ray diffraction, dotted line: neutron scattering).

temperature increases from 573 to 823 K indicating the phase transition of MNK eutectic, and the increase of intermolecular distance results in the decrease of density and shear viscosity.

Studies have shown that the addition of covalent salt MgCl_2 results in highly mismatched molecular size, shape, and bonding of different species for mixed chlorides [45]. Therefore, the evolution of equilibrium coordination structure of Mg^{2+} in MNK eutectic as a function of temperature is investigated as shown in Fig. 8. At 573 K, there are a few polyhedrons formed by Mg^{2+} -centered Cl clusters, and most of them are tetrahedrons (MgCl_4^{2-}) which had been detected by XRD patterns [46]. However, only two Cl atoms (Cl28 and Cl47) are bonded by two separated polyhedrons, that is not good for long-range ion transport. As temperature increasing from 623 to 723 K, both the numbers of shared Cl atoms and 5-fold coordination structures of Mg–Cl clusters increase. The number of Cl atoms by corner-sharing and edge-sharing is more than 10 when temperature is much higher than T_m (i.e., 773 and 823 K),

and the network structure is connected by alternating polyhedrons, which is conducive to the improvement of whole transport performance. It should be noted that the shared Cl atoms of 673 K (Cl29, Cl38, Cl56, and Cl57) are totally different from that of 873 K whose total diffusion coefficient is the largest. Therefore, it can be concluded that there exists a solid-liquid coexisting mixture when the temperature is close to T_m , and it is detrimental to ion diffusion as mentioned in Sections 3.2.1 and 3.3.2.

4. Conclusions

In this work, the FPMD simulations are proposed to predict thermophysical properties and to explain melting mechanism of MNK eutectic with the combination of experimental measurements. The specially designed thermodynamic cycle, by using the absolute energy of MNK eutectic at 0 K as ground state energy, successfully fulfills the calculations of latent heat energy related to ternary chlorides. Besides, the ab-initio approaches are applied to predict the specific heat capacities, ionic self-diffusion coefficients, and shear viscosities of MNK eutectic in terms of the fluctuation of free energy, mean square displacement, and Stokes-Einstein equation. The calculated thermal conductivities based on self-diffusion coefficients and isometric specific heat capacities obtained from FPMD simulations within NVT ensemble agree well with experimental measurements, and the evaluated viscosities are also reasonably consistent with predictive values from single component molten salt by additive contribution method. Meanwhile, the melting mechanism of MNK eutectic is elaborated in detail from the evolution of Mg^{2+} coordination structures where the connectivity of network-forming polyhedrons by Cl ions directly result in phase transition. Therefore, it is concluded that FPMD simulations can be a powerful tool to explore thermal properties of molten salts and their mixtures in the establishment of big data for thermodynamic, kinetic properties and structural characteristics. In addition, FPMD is also useful for the validation and explanation of experimental data and phenomenon to enhance the efficiency and cost competitiveness of future CSP systems.

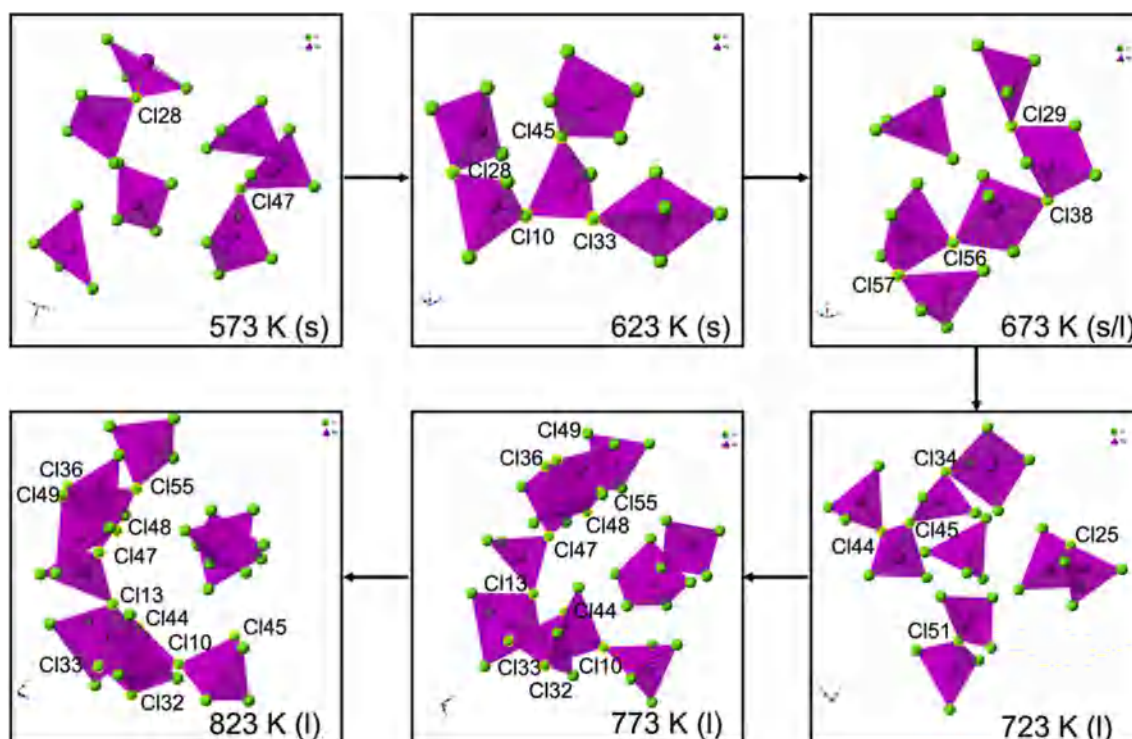


Fig. 8. Evolution of network-forming coordination structures of Mg^{2+} as a function of temperature (the shared Cl atoms are highlighted).

Declaration of competing interest

The authors declare that they have no known competing financial interests or personal relationships that could have appeared to influence the work reported in this paper.

CRedit authorship contribution statement

Xuejiao Li: Methodology, Software, Data curation, Formal analysis, Visualization, Writing - original draft. **Na Li:** Validation, Data curation, Investigation, Resources. **Weihua Liu:** Validation, Data curation, Investigation, Resources, Writing - review & editing. **Zhongfeng Tang:** Conceptualization, Writing - review & editing, Funding acquisition. **Jianqiang Wang:** Supervision, Project administration, Funding acquisition.

Acknowledgements

Supported by National Key R&D Program of China (No. 2018YFB1501002), Qinghai Major Science and Technology Projects (No. 2017-GX-A3), "Transformational Technologies for Clean Energy and Demonstration", Strategic Priority Research Program of the Chinese Academy of Sciences (No. XDA21000000).

Appendix A. Supplementary data

Supplementary data to this article can be found online at <https://doi.org/10.1016/j.solmat.2020.110504>.

References

- M. Mehos, C. Turchi, J. Vidal, M. Wagner, Z. Ma, C. Ho, W. Kolb, C. Andracka, A. Kruienza, Concentrating Solar Power Gen3 Demonstration Roadmap; NREL/TP-5500-67464, National Renewable Energy Lab.(NREL), Golden, CO (United States), 2017.
- P.D. Myers, D.Y. Goswami, Thermal energy storage using chloride salts and their eutectics, *Appl. Therm. Eng.* 109 (2016) 889–900.
- S. Ushak, A.G. Fernández, M. Grageda, 3-Using molten salts and other liquid sensible storage media in thermal energy storage (TES) systems, in: L.F. Cabeza (Ed.), *Advances in Thermal Energy Storage Systems*, Woodhead Publishing, 2015, pp. 49–63.
- X. Xu, G. Dehghani, J. Ning, P. Li, Basic properties of eutectic chloride salts NaCl-KCl-ZnCl₂ and NaCl-KCl-MgCl₂ as HTFs and thermal storage media measured using simultaneous DSC-TGA, *Sol. Energy* 162 (2018) 431–441.
- G. Mohan, M. Venkataraman, J. Gomez-Vidal, J. Coventry, Assessment of a novel ternary eutectic chloride salt for next generation high-temperature sensible heat storage, *Energy Convers. Manag.* 167 (2018) 156–164.
- H. Sun, J. Wang, Z. Li, P. Zhang, X. Su, Corrosion behavior of 316SS and Ni-based alloys in a ternary NaCl-KCl-MgCl₂ molten salt, *Sol. Energy* 171 (2018) 320–329.
- W. Ding, H. Shi, A. Jianu, Y. Xiu, A. Bonk, A. Weisenburger, T. Bauer, Molten chloride salts for next generation concentrated solar power plants: mitigation strategies against corrosion of structural materials, *Sol. Energy Mater. Sol. Cell.* 193 (2019) 298–313.
- W. Ding, H. Shi, Y. Xiu, A. Bonk, A. Weisenburger, A. Jianu, T. Bauer, Hot corrosion behavior of commercial alloys in thermal energy storage material of molten MgCl₂/KCl/NaCl under inert atmosphere, *Sol. Energy Mater. Sol. Cell.* 184 (2018) 22–30.
- Y. Yuan, W. Li, H. Chen, Z. Wang, X. Jin, G.Z. Chen, Electrolysis of metal oxides in MgCl₂ based molten salts with an inert graphite anode, *Faraday Discuss* 190 (2016) 85–96.
- S. Vandarkuzhali, P. Venkatesh, S. Ghosh, G. Seenivasan, B. Prabhakara Reddy, T. Subramanian, N. Sivaraman, K. Nagarajan, Electrochemistry of rare earth oxy ions REO⁺ (RE=Ce, La, Nd) in molten MgCl₂-NaCl-KCl eutectic, *J. Electroanal. Chem.* 611 (1) (2007) 181–191.
- J. Delhommelle, J. Petracic, Shear viscosity of molten sodium chloride, *J. Chem. Phys.* 118 (6) (2003) 2783–2791.
- M. Matsumiya, R. Takagi, A molecular dynamics simulation of the electric properties in molten chloride and fluoride quaternary systems, *Electrochim. Acta* 46 (23) (2001) 3563–3572.
- C. Robelin, P. Chartrand, Thermodynamic evaluation and optimization of the (NaCl+KCl+MgCl₂+CaCl₂+ZnCl₂) system, *J. Chem. Therm.* 43 (3) (2011) 377–391.
- N. Galamba, C.A. Nieto de Castro, J.F. Ely, Thermal conductivity of molten alkali halides from equilibrium molecular dynamics simulations, *J. Chem. Phys.* 120 (18) (2004) 8676–8682.
- N. Galamba, C. Nieto de Castro, J. Ely, Molecular dynamics simulation of the shear viscosity of molten alkali halides, *J. Phys. Chem. B* 108 (2004) 3658–3662.
- J. Wang, Z. Sun, G. Lu, J. Yu, Molecular dynamics simulations of the local structures and transport coefficients of molten alkali chlorides, *J. Phys. Chem. B* 118 (34) (2014) 10196–10206.
- J. Wang, J. Wu, Z. Sun, G. Lu, J. Yu, Molecular dynamics study of the transport properties and local structures of molten binary systems (Li, Na)Cl, (Li, K)Cl and (Na, K)Cl, *J. Mol. Liq.* 209 (2015) 498–507.
- N. Galamba, B.J. Costa Cabral, First principles molecular dynamics of molten NaCl, *J. Chem. Phys.* 126 (12) (2007) 124502.
- G. Kresse, J. Furthmüller, Efficiency of ab-initio total energy calculations for metals and semiconductors using a plane-wave basis set, *Comput. Mater. Sci.* 6 (1) (1996) 15–50.
- G. Kresse, J. Furthmüller, Efficient iterative schemes for ab initio total-energy calculations using a plane-wave basis set, *Phys. Rev. B* 54 (16) (1996) 11169–11186.
- G. Kresse, J. Hafner, Ab initio molecular dynamics for liquid metals, *Phys. Rev. B* 47 (1) (1993) 558–561.
- J.P. Perdew, K. Burke, M. Ernzerhof, Generalized gradient approximation made simple, *Phys. Rev. Lett.* 77 (18) (1996) 3865–3868.
- G. Kresse, D. Joubert, From ultrasoft pseudopotentials to the projector augmented-wave method, *Phys. Rev. B* 59 (3) (1999) 1758–1775.
- P.E. Blöchl, Projector augmented-wave method, *Phys. Rev. B* 50 (24) (1994) 17953–17979.
- X. Li, J. Song, S. Shi, L. Yan, Z. Zhang, T. Jiang, S. Peng, Dynamic fluctuation of U³⁺ coordination structure in the molten LiCl-KCl eutectic via first principles molecular dynamics simulations, *J. Phys. Chem.* 121 (3) (2017) 571–578.
- S. Nosé, A unified formulation of the constant temperature molecular dynamics methods, *J. Chem. Phys.* 81 (1) (1984) 511–519.
- S. Nosé, A molecular dynamics method for simulations in the canonical ensemble, *Mol. Phys.* 52 (2) (1984) 255–268.
- M. Parrinello, A. Rahman, Polymorphic transitions in single crystals: a new molecular dynamics method, *J. Appl. Phys.* 52 (12) (1981) 7182–7190.
- X. Li, Y. Wang, S. Wu, L. Xie, Preparation and investigation of multicomponent alkali nitrate/nitrite salts for low temperature thermal energy storage, *Energy* 160 (2018) 1021–1029.
- X. An, J. Cheng, P. Zhang, Z. Tang, J. Wang, Determination and evaluation of the thermophysical properties of an alkali carbonate eutectic molten salt, *Faraday Discuss* 190 (2016) 327–338.
- P. Zhang, J. Cheng, Y. Jin, X. An, Evaluation of thermal physical properties of molten nitrate salts with low melting temperature, *Sol. Energy Mater. Sol. Cell.* 176 (2018) 36–41.
- X. An, J. Cheng, H. Yin, L. Xie, P. Zhang, Thermal conductivity of high temperature fluoride molten salt determined by laser flash technique, *Int. J. Heat Mass Tran.* 90 (2015) 872–877.
- A. Belonoshko, R. Ahuja, B. Johansson, Molecular dynamics of LiF melting, *Phys. Rev. B* 61 (2000) 11928–11935.
- T. Bucko, F. Šimko, On the structure of crystalline and molten cryolite: insights from the ab initio molecular dynamics in NpT ensemble, *J. Chem. Phys.* 144 (6) (2016), 064502.
- C. Robelin, P. Chartrand, G. Eriksson, A density model for multicomponent liquids based on the modified quasicheical model: application to the NaCl-KCl-MgCl₂-CaCl₂ system, *Metall. Mater. Trans. B* 38 (6) (2007) 869–879.
- M.M. Kenisarin, High-temperature phase change materials for thermal energy storage, *Renew. Sustain. Energy Rev.* 14 (3) (2010) 955–970.
- L.H. Xiong, X.D. Wang, Q.P. Cao, D.X. Zhang, H.L. Xie, T.Q. Xiao, J.Z. Jiang, Composition- and temperature-dependent liquid structures in Al-Cu alloys: an ab initio molecular dynamics and x-ray diffraction study, *J. Phys. Condens. Matter* 29 (3) (2017), 035101.
- T. Aguilar, J. Navas, A. Sánchez-Coronilla, E.I. Martín, J.J. Gallardo, P. Martínez-Merino, R. Gómez-Villarejo, J.C. Piñero, R. Alcántara, C. Fernández-Lorenzo, Investigation of enhanced thermal properties in NiO-based nanofluids for concentrating solar power applications: a molecular dynamics and experimental analysis, *Appl. Energy* 211 (2018) 677–688.
- V.R. Manga, S. Bringuier, J. Paul, S. Jayaraman, P. Lucas, P. Deymier, K. Muralidharan, Molecular dynamics simulations and thermodynamic modeling of NaCl-KCl-ZnCl₂ ternary system, *Calphad* 46 (2014) 176–183.
- V.R. Manga, N. Swintek, S. Bringuier, P. Lucas, P. Deymier, K. Muralidharan, Interplay between structure and transport properties of molten salt mixtures of ZnCl₂-NaCl-KCl: a molecular dynamics study, *J. Chem. Phys.* 144 (9) (2016) 176.
- J. Ding, G. Pan, L. Du, J. Lu, W. Wang, X. Wei, J. Li, Molecular dynamics simulations of the local structures and transport properties of Na₂CO₃ and K₂CO₃, *Appl. Energy* 227 (2018) 555–563.
- R. Vuilleumier, A. Seitsonen, N. Sator, B. Guillot, Structure, equation of state and transport properties of molten calcium carbonate (CaCO₃) by atomistic simulations, *Geochim. Cosmochim. Acta* 141 (2014) 547–566.
- D. Corradini, F.-X. Coudert, R. Vuilleumier, Insight into the Li₂CO₃-K₂CO₃ eutectic mixture from classical molecular dynamics: thermodynamics, structure, and dynamics, *J. Chem. Phys.* 144 (10) (2016) 104507.

- [44] G.J. Janz, C.B. Allen, N.P. Bansal, R.M. Murphy, R.P.T. Tomkins, Physical Properties Data Compilations Relevant to Energy Storage II. Molten Salts: Data on Single and Multi-Component Salt Systems, Troy, New York, 1979, pp. 49–81.
- [45] Y. Li, X. Xu, X. Wang, P. Li, Q. Hao, B. Xiao, Survey and evaluation of equations for thermophysical properties of binary/ternary eutectic salts from NaCl, KCl, MgCl₂, CaCl₂, ZnCl₂ for heat transfer and thermal storage fluids in CSP, Sol. Energy 152 (2017) 57–79.
- [46] J. Wang, H. Zhou, R. Zhong, S. Chen, Y. Deng, C. Liu, X. Sun, Corrosion behavior and mechanism of Fe-14Cr-Mn alloy in molten eutectic NaCl-MgCl₂ at different temperatures, Rare Met. Mater. Eng. 46 (4) (2017) 935–941.